

A satellite-derived baseline of photosynthetic life across Antarctica

Received: 5 December 2023

Accepted: 25 June 2024

Published online: 6 August 2024

 Check for updates

Charlotte V. Walshaw¹✉, Andrew Gray^{1,2}✉, Peter T. Fretwell³,
Peter Convey³, Matthew P. Davey⁴, Joanne S. Johnson³ &
Claudia Colesie¹✉

Terrestrial vegetation communities across Antarctica are characteristically sparse, presenting a challenge for mapping their occurrence using remote sensing at the continent scale. At present there is no continent-wide baseline record of Antarctic vegetation, and large-scale area estimates remain unquantified. With local vegetation distribution shifts now apparent and further predicted in response to environmental change across Antarctica, it is critical to establish a baseline to document these changes. Here we present a 10 m-resolution map of photosynthetic life in terrestrial and cryospheric habitats across the entire Antarctic continent, maritime archipelagos and islands south of 60° S. Using Sentinel-2 imagery (2017–2023) and spectral indices, we detected terrestrial green vegetation (vascular plants, bryophytes, green algae) and lichens across ice-free areas, and cryospheric green snow algae across coastal snowpacks. The detected vegetation occupies a total area of 44.2 km², with over half contained in the South Shetland Islands, altogether contributing just 0.12% of the total ice-free area included in the analysis. Due to methodological constraints, dark-coloured lichens and cyanobacterial mats were excluded from the study. This vegetation map improves the geospatial data available for vegetation across Antarctica, and provides a tool for future conservation planning and large-scale biogeographic assessments.

Ice-free habitats in Antarctica (comprising 0.2–0.5% of the total area of the continent^{1,2}) are dominated by cryptogamic communities, including bryophytes, lichens, algae and cyanobacteria³ (Fig. 1). Only two native species of vascular plant occur, both restricted to the western Antarctic Peninsula, South Shetland and South Orkney archipelagos, as well as the more northern sub-Antarctic islands³. Coastal snowpacks, where melt occurs during the summer months, also contain a considerable biomass in the form of microalgal blooms^{4,5} (Fig. 1f,g). Antarctic vegetation is extremely well adapted to survive the harsh environment⁶, and each type plays a locally important role in carbon and nutrient cycling^{5,7}. The environmental sensitivity of cryptogams also makes them excellent

bioindicators of regional climate change⁶. Therefore, mapping their presence across the minimally disturbed and abiotic-driven landscape in Antarctica could facilitate predictions of changing cryptogam cover in response to climate across other parts of the globe. For example, in the Arctic tundra biome, which is currently threatened by accelerated surface warming and species redistributions, and where ecological change attribution is complicated by both anthropogenic disturbance and more complex biological interactions⁸.

Vegetation across Antarctica is typically sparse⁹, with patch sizes ranging from less than tens of mm² to hundreds of m² (Fig. 1). The maritime Antarctic (land area north of the Gressitt Line at the base of the

¹School of Geosciences, Global Change Institute, University of Edinburgh, Edinburgh, UK. ²Terrestrial Ecology Section, Norwegian Institute for Nature Research (NINA), Oslo, Norway. ³British Antarctic Survey (BAS), Cambridge, UK. ⁴Scottish Association for Marine Science (SAMS), Oban, UK.

✉e-mail: Charlotte.Walshaw@ed.ac.uk; andrew.gray@nina.no; Claudia.Colesie@ed.ac.uk

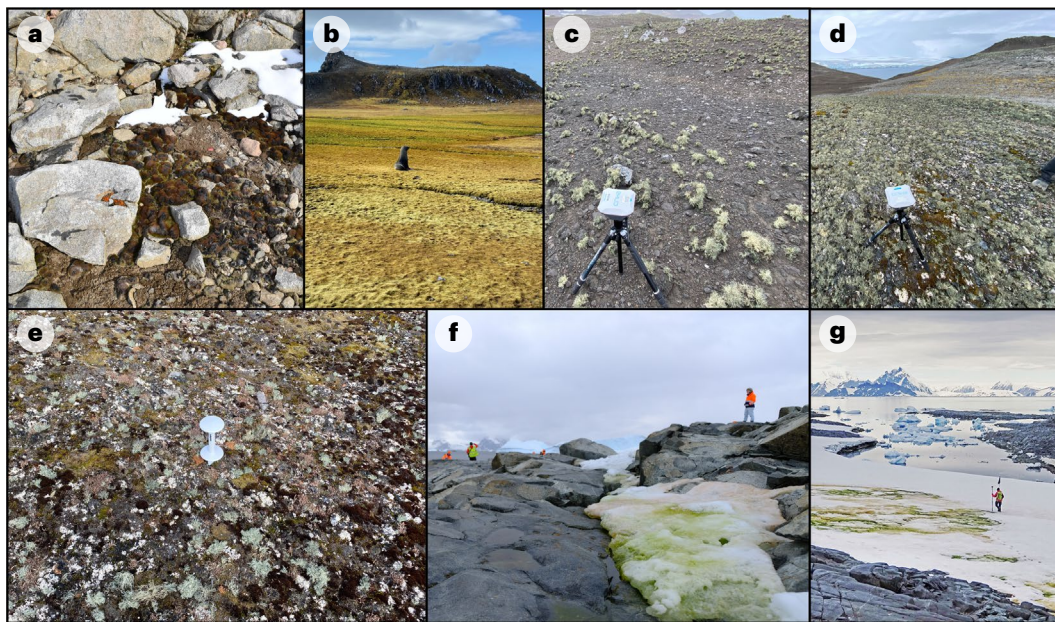


Fig. 1 | Examples of Antarctic vegetation. a–e, Terrestrial vegetation. **a**, Small patch of green/brown/black moss (*Bryum* sp.), $-1 \times 1 \text{ m}^2$ among boulders in Botany Bay (77° S ; continental Antarctic). **b**, Large carpet of moss (*Sanionia uncinata*) on Robert Island, South Shetland Islands (62° S ; maritime Antarctic). **c**, Sparse lichen (*Usnea* sp.) covering bare ground on Robert Island. **d**, Dense patch of predominantly lichen (*Usnea* sp.), with scattered moss (*Polytrichum* sp.), on Robert Island. **e**, Mixed fellfield of lichen (for example, *Usnea* sp. and orange

Sphaerophorus globosus) and moss (for example, green *Sanionia uncinata* and dark brown *Andreaea* sp.) on Robert Island. **f, g**, Cryospheric vegetation. **f**, Small bloom of green and red snow algae, $-1 \times 3 \text{ m}^2$, on Rothera Point, Ryder Bay, Adelaide Island (67° S ; maritime Antarctic). **g**, Large bloom of green and red snow algae, $-50 \times 100 \text{ m}^2$, Anchorage Island, Ryder Bay (67° S ; maritime Antarctic). Credit: **f**, A. Thomson.

Antarctic Peninsula¹⁰), and specifically the western Antarctic Peninsula and offshore island archipelagos, hosts more spatially extensive and diverse photosynthetic communities than the continental Antarctic (land south of the Gressitt Line, forming the main body of the continent¹⁰), due to higher mean summer air temperatures and water availability¹¹. Coastal oases such as the Windmill Islands ($66^\circ 16' \text{ S } 110^\circ 31' \text{ E}$) and Cape Hallett ($72^\circ 19' \text{ S } 170^\circ 16' \text{ E}$) provide exceptions, with relatively well-developed and extensive terrestrial vegetation^{12,13}, although with much lower biodiversity and biomass than in the maritime Antarctic. As quantitative information on vegetation cover across Antarctica is mostly limited to a small number of local baseline assessments^{14–17}, large-scale vegetation distribution maps will be critical for informing conservation strategies for Antarctica's terrestrial biodiversity, which is inadequately protected under the existing Antarctic Specially Protected Area (ASPA) system^{18–20}. In recent decades, surface air temperatures in the western Antarctic Peninsula have warmed around three times faster than the global average¹⁷. This has been associated with small but significant shifts in the spatial distribution and growth patterns of terrestrial vegetation, particularly the two native flowering plants¹⁷. Following a brief hiatus early in the twenty-first century²¹, this warming is predicted to continue alongside an increase in the frequency and intensity of rainfall events along the Antarctic coastline²². Associated changes in moisture availability will lead to further alterations in both the structure and functioning of Antarctica's vegetation²³. Under current 'business as usual' warming scenarios applied to Antarctica, predicted ice melt could expand the area of available ice-free ground by 25% across the entire continent, and -300% in the Antarctic Peninsula region^{2,24}. This would result in more terrestrial habitat becoming available for biological colonization²⁴, emphasizing the urgent need for baseline information to identify and document these predicted future changes.

The size of Antarctica (>12 million km^2) and its inaccessibility necessitate a remote-sensing framework to map photosynthetic life at the continent scale. The European Space Agency Sentinel-2 satellite constellation offers multispectral imagery across much of the continent, at a weekly interval and at medium spatial resolution (up to

Table 1 | Summary of key results

Vegetation type	Terrestrial		Cryospheric
	Green vegetation (vascular plants, bryophytes, green algae)	Lichen	Green snow algae
Total area (km^2)	32.8 (17.1)	8.1 (6.4)	3.3 (0.4)
Maritime Antarctic (km^2)	27.2 (14.1)	7.9 (6.2)	2.3 (0.3)
Continental Antarctic (km^2)	5.6 (3.0)	0.2 (0.2)	1.0 (0.1)
Minimum area for detection (m^2)	52	79	11
Accuracy assessment (Cohen's kappa statistic)	Total (0.62)		Total (0.69)

Total area: maximum area of detected vegetation (in km^2) across Antarctica, in addition to the area of detected vegetation in the maritime and continental Antarctic, between 2017 (for green snow algae) or 2018 (terrestrial vegetation) and 2023. Values in parentheses denote the lower bound of total area estimates in km^2 . Minimum area for detection: the minimum estimated area (in m^2) that each vegetation type must occupy within a Sentinel-2 pixel for detection. Accuracy assessment: Cohen's kappa statistic for green vegetation ($n=254$), lichen ($n=57$) and bare ground ($n=144$) validation sites, and for green snow algae and bare snow ($n=256$) validation sites across coastal snowpacks (Extended Data Fig. 1).

10 m/pixel). Efforts to utilize the capability of Sentinel-2 for detecting and discriminating Antarctic terrestrial vegetation have thus far been limited^{25–27}, and only one study has focused on mapping at the regional scale across the northern Antarctic Peninsula²⁵. Earlier attempts at mapping across the Antarctic Peninsula were conducted using Landsat imagery (30 m/pixel)^{28,29} but, given the patchiness of Antarctic vegetation, these studies highlighted the need for higher-resolution imagery. Satellite remote sensing of Antarctic snow algal blooms has so far been limited to areas on the Antarctic Peninsula, focusing largely on green blooms^{5,30–32}.

In this study we used spectral indices from Sentinel-2 imagery to map terrestrial green vegetation (vascular plants, bryophytes and

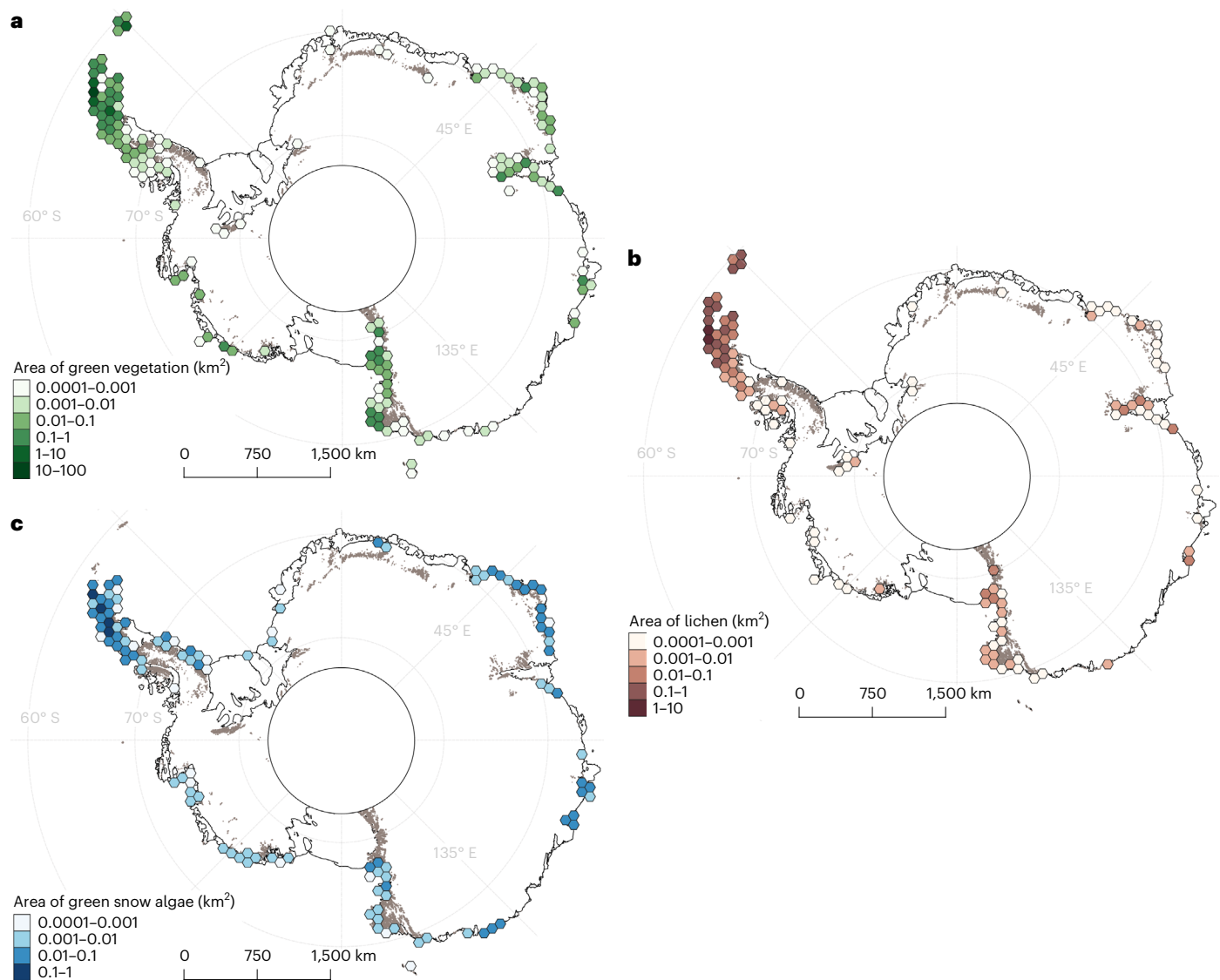


Fig. 2 | Area of photosynthetic life detected in Sentinel-2 imagery, visualized within individual 100-km hexagonal grids. a, b, Terrestrial vegetation: green vegetation (vascular plants, bryophytes and green algae) (a) and lichens (b). c, Cryospheric vegetation (green snow algae). Areas within individual hexagonal grids were derived from respective cumulative vegetation pixel (10 × 10 m)

counts. Ice-free areas (not to scale) are shown in grey shading underlying the hexagonal grids. The ‘polar hole’ is displayed south of 82.8° S, where no imagery was available. The Antarctic coastline and ice-free area layers were retrieved from the Antarctic Digital Database Version 7.0 (<http://www.add.scar.org/>).

green algae), lichens and cryospheric green snow algae across the entire Antarctic continent and maritime islands south of 60° S. We grouped vascular plants, bryophytes and green algae together as green vegetation for remote detection with the normalized difference vegetation index (NDVI), a spectral measure of vegetation greenness. However, these vegetation types are not constantly green, and species identity, environmental conditions and life-cycle stage can all induce brown colouration, still detectable with NDVI (Supplementary Table 1). Therefore, we included brown-coloured vegetation within the green vegetation class. Although common, vegetation in aquatic habitats (such as lakes and stream channels)^{9,23} was excluded from this study (Methods).

Area estimates of vegetation across Antarctica

Our map detected vegetation across Antarctica covering a total area of 44.2 km² (data from 2017–2023). The combined area of terrestrial vegetation accounts for just 0.12% of the total ice-free area included in our analysis (Methods). A large majority of the detected vegetation

was present in the maritime Antarctic (84.8%; Fig. 2), including 83% of all green vegetation (vascular plants, bryophytes and green algae), 98% of all lichens and 70% of all green snow algae (Table 1). Green snow algae contributed 7.5% of the total area of detected vegetation (Table 1), and displayed a similar distribution pattern across the continent to terrestrial vegetation (Fig. 2). However, green snow algae were also detected growing in isolated patches on ice shelves, often in locations close to emperor penguin colonies³³, such as on the Larsen Ice Shelf close to the Dolleman colony (East Antarctic Peninsula) and on the Ronne Ice Shelf close to the Smith and Gould colonies (west of Ellsworth Land; Fig. 3). Roughly 40% of all green vegetation and lichens in ice-free areas were detected within 5 km of Antarctica’s Important Bird Areas (IBAs), such as on the Seabee Hook in Cape Hallett (North Victoria Land) and on Shirley Island in the Windmill Islands, both of which support large Adélie penguin colonies³⁴ (Fig. 3). These findings support the spatial association between vegetation and bird colonies^{5,35}, and future applications of the mapping can explore large-scale biogeographic associations in detail and facilitate the identification of previously unknown IBAs.

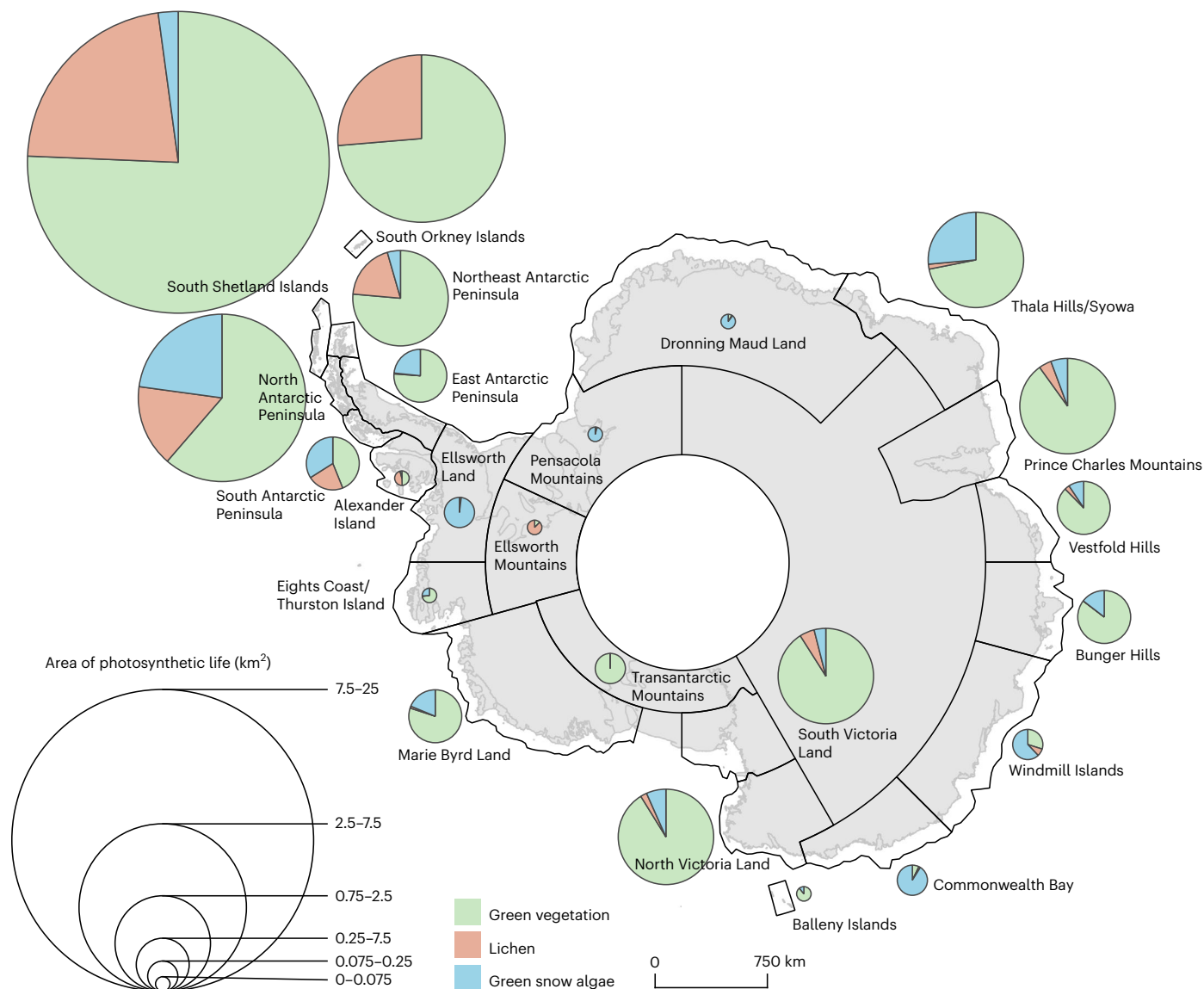


Fig. 3 | Vegetation within Antarctica's expert-defined bioregions. The total area of vegetation (not to scale) detected within each bioregion (black outlines), displayed by the relative size of the pie charts, which are scaled by the median value of each interval range. The proportion of green vegetation, lichens and green snow algae in each bioregion is shown within the pie charts. The polar

hole is displayed south of 82.8° S, where no imagery was available. The Antarctic coastline layer was retrieved from the Antarctic Digital Database Version 7.0 (<http://www.add.scar.org/>) and the bioregion layer from https://data.aad.gov.au/aadc/biodiversity/index_regions.cfm.

The minimum area of vegetation required for detection within a Sentinel-2 pixel (100 m²) differed based on the specific vegetation type (Table 1) and its degree of spectral separability from the background pixel constituent. The classification model sensitivity was highest for green snow algae, for which blooms could be detected at patch sizes covering just one-tenth of a pixel (11 m²) due to the high contrast in spectral reflectance between largely white snow and green algae. This was followed by terrestrial green vegetation, which was required to occupy at least half of one pixel (52 m²) for detection. Lichen was the most difficult vegetation type to detect due to its relatively low contrast in spectral reflectance with bare ground (Supplementary Table 1), and required occupancy of over three-quarters of a pixel (79 m²) for detection. Consequently, smaller areas of green snow algae could be detected relative to green vegetation and lichen. Any patches of vegetation that were below the respective detection limits (Table 1) could not be mapped, resulting in an underestimation of the total area of vegetation across Antarctica. However, the results do give a consistent and comparable metric across the continent.

There was substantial agreement between the remote-sensed terrestrial and cryospheric vegetation and the in situ validation data ($\kappa = 0.62$ and $\kappa = 0.69$, respectively; Table 1 and Extended Data Fig. 1). Nevertheless, false positives in the mapping occurred both in the continental and maritime Antarctic. Notably, across Taylor Valley in South Victoria Land (Fig. 3), confirmed areas of cyanobacterial mat presence (for example, within meltwater streams of Canada and Howard Glacier)^{36–38}, which we were unable to discriminate as a separate class, were detected by our model as green vegetation (Methods). Similarly, based on overlap analysis with station footprints³⁹, we estimated that 0.01 km² of false positives arose from research station infrastructure, which in some cases were erroneously detected as terrestrial vegetation.

Snow algae false positives were predominantly a result of mixed pixels, crevassed ice and, in the case of areas around James Ross Island and the Dry Valleys (South Victoria Land, Fig. 3), mineral debris within the snowpack. Mineral debris in snow did not cause false positives for green snow algae in other areas, and we suggest that this relates to the mineral composition in these regions or that there is a genuine

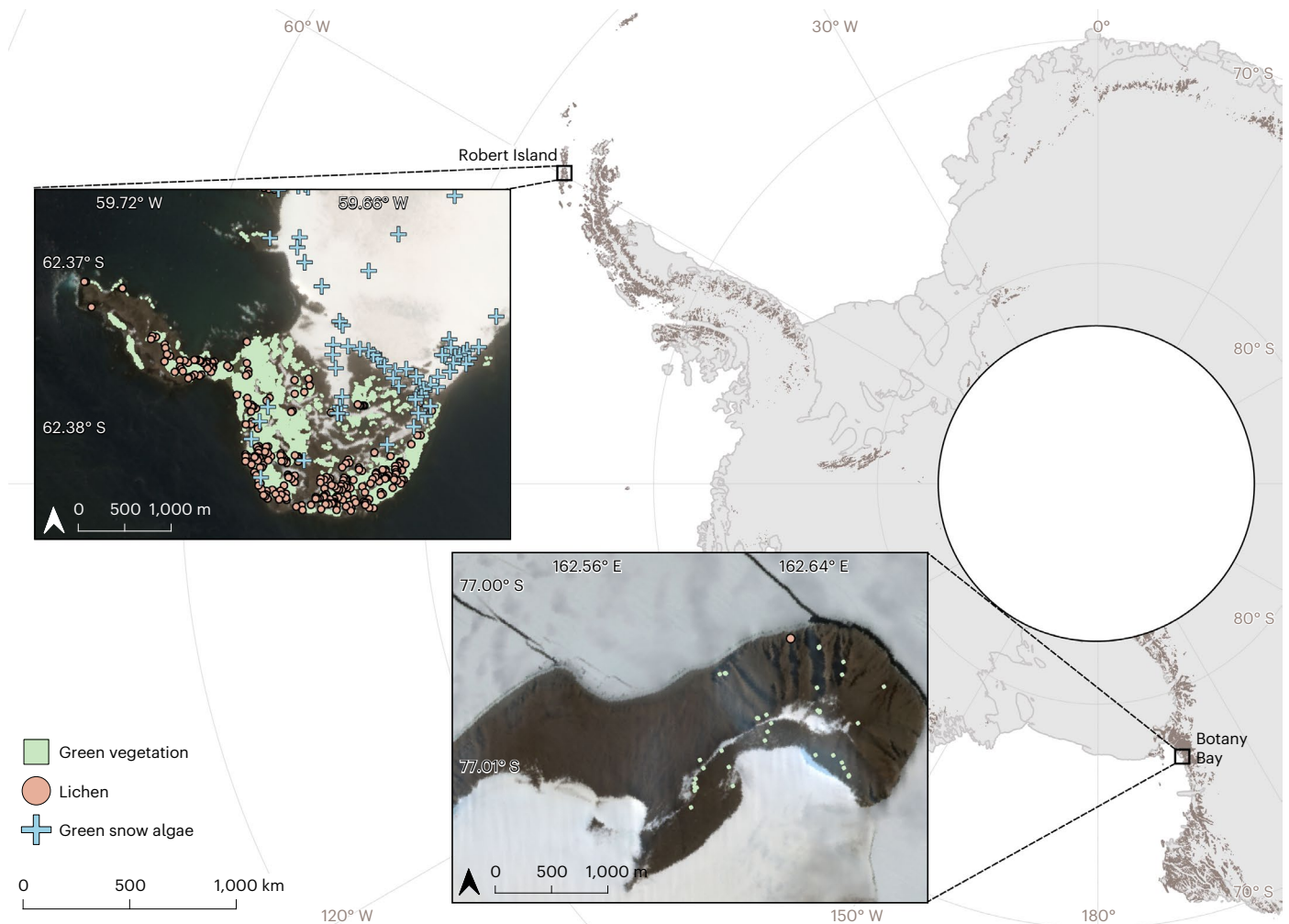


Fig. 4 | Contrast in detected vegetation between Robert Island (maritime Antarctic) and Botany Bay (continental Antarctic). Top left inset: vegetation pixels (not to scale) detected by our mapping in the southernmost part of Robert Island (South Shetland Islands), overlaying an optimized Sentinel-2 composite from January 2023. Bottom centre inset: vegetation pixels (not to scale) detected

by our mapping in Botany Bay (South Victoria Land), overlaying an optimized Sentinel-2 minimum composite from January–February 2023. The ‘polar hole’ is displayed south of 82.8° S. Ice-free areas in dark grey (not to scale) and base maps were retrieved from the Antarctic Digital Database Version 7.0.

presence within the snow. Until this can be verified, we masked these areas from our analysis. Marine algal blooms within mobile pack ice, as well as overturned icebergs, also generated some false positives in areas where sea ice persisted over the timeframe of the analysed imagery. These errors should reduce in frequency in the future as more imagery is incorporated into processing. For the purposes of this analysis, they were removed manually. Red snow algal blooms and ice algae are also known to be present, but were not reliably discriminated from mineral debris using Sentinel-2 imagery.

Vegetation within the Antarctic bioregions

The expert-defined biogeographic regions (bioregions) of Antarctica provide a spatial characterization of biodiversity patterns alongside the Antarctic Conservation Biogeographic Regions (ACBR), with the latter only including ice-free areas^{2,40}. We present quantitative estimates of the total area and spatial coverage of terrestrial and cryospheric vegetation within these bioregions (Fig. 3). This will serve as a complementary dataset to the ACBR² and Antarctic Terrestrial Biodiversity Database⁴¹ for informing future conservation strategies for Antarctica’s terrestrial biodiversity. Our analysis showed that over half of all detected terrestrial vegetation (55%, 24.2 km²) was present in the South Shetland Islands, including 56% of all green vegetation, 66% of all lichens and 16% of all green snow algae (Extended Data Table 1). Conversely, the

Ellsworth Mountains contained the smallest detected area of vegetation (0.006%, 0.002 km²), of which lichen contributed the largest proportion (87.5%). In the North Antarctic Peninsula bioregion, we detected the largest area of green snow algae (40%). Generally, green snow algae dominated in bioregions where terrestrial vegetation was comparatively sparse, including Ellsworth Land, Pensacola Mountains, Dronning Maud Land and Commonwealth Bay (Fig. 3). This could possibly be explained by model detection limit constraints (Table 1) restricting the detection of terrestrial vegetation in these regions, as well as the close proximity of snow algal blooms to penguin colonies.

Challenges of mapping sparse vegetation

The medium spatial resolution of Sentinel-2 imagery posed a challenge for detecting Antarctica’s sparse vegetation, and a pronounced contrast was apparent in the detected area of vegetation between the maritime and continental Antarctic. By comparing two locations generally accepted to be ‘well vegetated’ in their respective regional contexts, our mapping detected 1.5 km² of vegetation across the southernmost part of Robert Island (62° 24’ S 59° 30’ W) in the South Shetland Islands and 0.0038 km² across Botany Bay (77° 00’ S 162° 32’ E) in South Victoria Land (Fig. 4). Although ground validation confirmed that Robert Island hosts more spatially extensive vegetation (Fig. 1b,d) than Botany Bay (Fig. 1a), the high diversity and abundance of lichens and

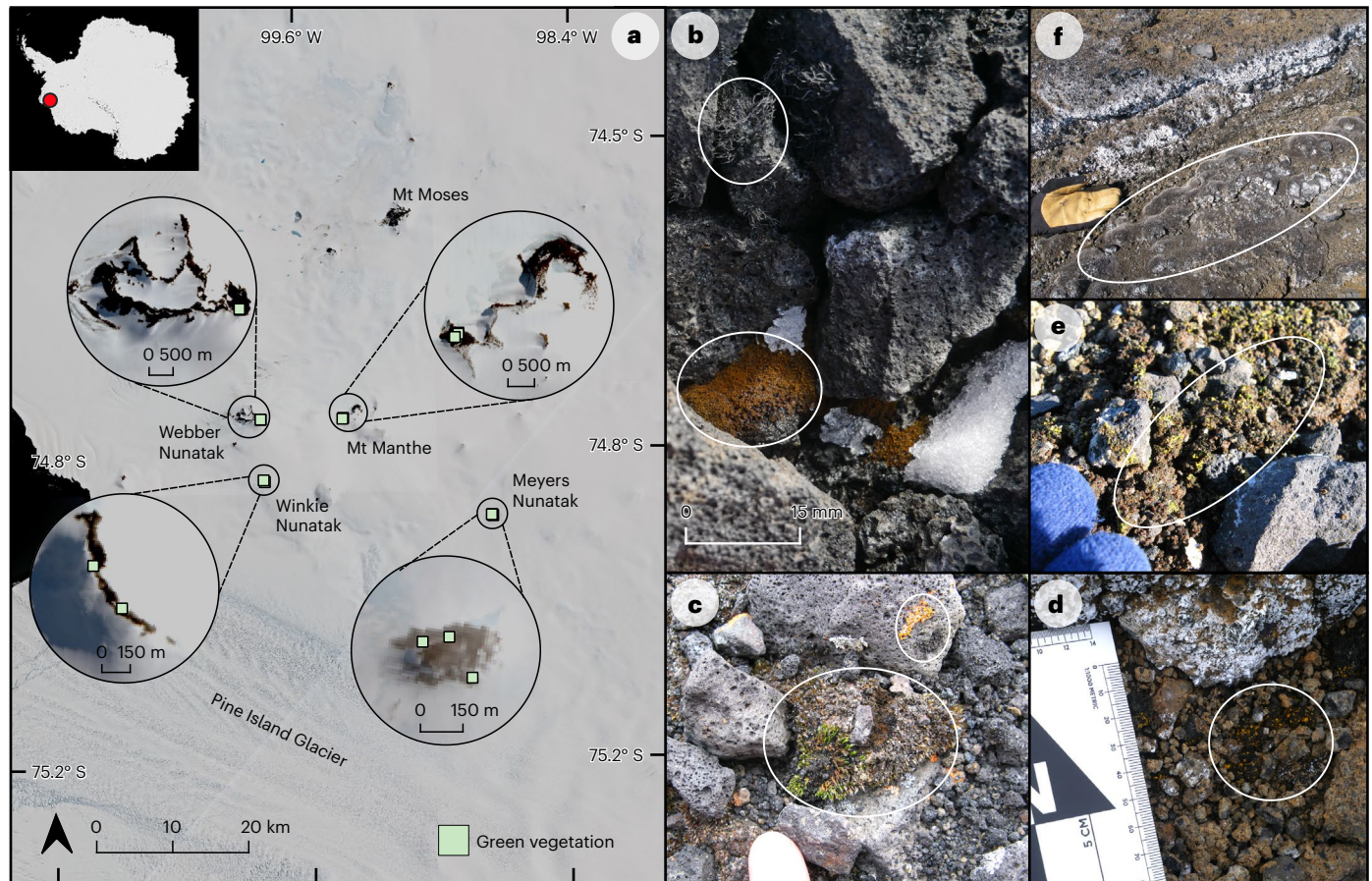


Fig. 5 | Vegetation observed on nunataks in the Hudson Mountains.

a, Sentinel-2 composite imagery (December 2019–February 2020) displaying green vegetation pixels (not to scale) detected on Webber Nunatak (74° 47' S 99° 50' W; top left inset), Winkie Nunatak (74° 51' S 99° 46' W; bottom left inset), Mount Manthe (74° 47' S 99° 21' W; top right inset) and Meyers Nunatak (74° 54' S 99° 46' W; bottom right inset). The inset in the top corner of the panel shows the location of the Hudson Mountains (72° 25' S 99° 30' W; red circle) with MODIS

imagery. **b–f**, Digital photographs of lichen and moss species (circled) on the Hudson Mountain nunataks (November–December 2019): brown moss and black lichen (Winkie Nunatak) (**b**); orange lichen and brown/green moss (Webber Nunatak; finger for scale) (**c**); orange lichen growing on brown moss (Mount Manthe) (**d**); lichen and possible moss (Meyers Nunatak; gloved fingers for scale) (**e**); grey moss (Mount Moses; glove for scale) (**f**). Credit: **b, d**, T. King, British Antarctic Survey.

mosses at Botany Bay^{42,43} relative to other continental sites is not well represented by the map, due to their presence primarily below model detection limits (Table 1). This highlights the bias in our map towards positive detection in the maritime Antarctic, where vegetation extent is generally greater and more likely to exceed minimum detection limits. As a consequence, the map systematically underestimates the area of patchy vegetation existing below detection limits across Antarctica. This effect was especially pronounced for the lichen mapping (Figs. 2 and 3), where high minimum area requirements for detection (79 m²) restricted the ability to map this typically patchy group. Future method development is required to include the probably significant area of lichens (and cyanobacterial mats) that could not be detected. Uncertainty in green snow algae area estimates, aside from blooms that were of lower cell abundance than our detection limits, resulted from blooms that were obscured by snow at the time of image acquisition.

Using Landsat Enhanced Thematic Mapper imagery and NDVI thresholding, a previous regional vegetation mapping study detected 44.6 km² of terrestrial vegetation across Graham Land (northern Antarctic Peninsula)²⁸. This is 3.7 km² more than our terrestrial vegetation estimate across the entire Antarctic and 9.5 km² more than our maritime Antarctic estimate (Table 1). However, the larger footprint of Landsat imagery (30 × 30 m) reduces its ability to characterize heterogeneous vegetation, with a larger spatial contribution from non-vegetated sub-pixel components appearing as propagated errors within the final area estimate. The use of a low minimum NDVI threshold value (0.05)

also increased the occurrence of rock false positives²⁸. For example, in the Finlandia Foothills (69° 56' S 70° 9' W) on Alexander Island, investigation of relatively high NDVI pixels (up to 0.15), which were thought to be vegetation, were shown to be haematite when visited by British Antarctic Survey field scientists in 2018 (Supplementary Table 2). Further inspection of ground-measured reflectance revealed that the local rock types had NDVI values ranging from 0.05 to 0.22 (Supplementary Table 1). Relatively high NDVI values from oxidized granite have also recently been recorded in the McMurdo Dry Valleys (South Victoria Land)⁴⁴. In our study, the reduced spectral influence from non-vegetated sub-pixel components in higher-resolution Sentinel-2 imagery enabled the use of higher minimum NDVI thresholds (0.2; Extended Data Table 2). This, in turn, reduced the occurrence of rock false positives across the Finlandia Foothills, without generating large relative increases in vegetation false negatives (which was found to be the case in Landsat imagery²⁸). Further investigation is required, perhaps utilizing the next generation of hyperspectral satellites, to comprehensively evaluate the performance of our model with respect to rock false positives for different geologies across Antarctica.

Previous mapping of green snow algal blooms on the Antarctic Peninsula indicated that Sentinel-2 probably underestimated algal bloom area by up to 17.5 times, mostly by excluding blooms of red algae from analysis, which are also common along the Antarctic coastline³⁰. Unlike terrestrial vegetation, we saw little difference in the characteristic bloom morphology of green snow algae between the maritime and continental

Antarctic, with blooms primarily forming on small islands, snow-covered rocky outcrops and at the foot of slopes. This was reflected by similar kappa validation scores (0.61 and 0.60, respectively), indicating similar detection performance across both regions. The combined area of green snow algae for Antarctica, as presented here (3.3 km²), greatly increases the Peninsula-only estimates (1.9 km²) made between 2017 and 2019 (ref. 5). This finding indicates that green snow algal blooms comprise a substantial proportion of vegetation in Antarctica's cryosphere.

Sentinel-2 is too spatially coarse to confidently map the small, patchy and heterogeneous areas of Antarctic vegetation using spectral indices. Previous work has explored the use of spectral unmixing techniques^{29,45,46} and combining multi-resolution imagery^{27,47} at selected sites across Antarctica to overcome this limitation of resolution. However, further investigation into minimizing within-class (and optimizing between-class) spectral reflectance variability is required, alongside increased availability of imagery from higher-resolution satellites and unoccupied aerial vehicles (UAVs).

Revealing new areas of conservation interest

The synoptic view provided with this vegetation map now offers the ability to identify and map new areas of conservation interest across Antarctica, particularly in more inaccessible and biologically data-poor locations. One example is the Hudson Mountains in the Amundsen Sea sector, which consist of a series of small volcanic nunataks protruding through the West Antarctic Ice Sheet (Fig. 5a). Biological records for the Hudson Mountains are sparse, with limited surveys undertaken during the 1968/1969⁴⁸, 2007/2008⁴⁹, 2009/2010⁴⁹ and 2019/2020 seasons (Supplementary Table 2). Scattered lichens have been reported on 14 nunataks, including *Usnea antarctica* on Mount Moses (Fig. 5a), and moss communities growing in rock cracks on a smaller number of nunataks^{48,49}. Lichen and moss presence on some of the nunataks was also recently confirmed by a British Antarctic Survey geological field party (Fig. 5b–f and Supplementary Table 2). However, information on the spatial distribution and coverage of vegetation in these regions remains largely qualitative and incomplete. Our remote mapping identified small areas of green vegetation on Webber Nunatak (306 m²), Winkie Nunatak (204 m²), Meyers Nunatak (306 m²) and Mount Manthe (714 m²) (Fig. 5a). The latter two are consistent with the location of moss observed in November and December 2019 (Supplementary Table 2). However, observations also revealed the presence of false negatives in the remote detection of lichens and mosses on these nunataks, as well as on Mount Moses (Fig. 5). Apart from detection limit constraints restricting the remote identification of small patches of lichens and mosses (Fig. 5b–f), the false negatives may also result from dark-coloured lichens (for example, Fig. 5b) and grey or black mosses (for example, Fig. 5f), which are likely to have very low reflectance signals in visible wavelengths⁵⁰. Nevertheless, the coincidence of remote detections and field observations demonstrates an important application of our remote mapping for identifying ecologically rich areas of terrestrial and cryospheric vegetation, for long-term monitoring in areas which often lack comprehensive baseline surveys and are seldom visited by terrestrial biologists.

Online content

Any methods, additional references, Nature Portfolio reporting summaries, source data, extended data, supplementary information, acknowledgements, peer review information; details of author contributions and competing interests; and statements of data and code availability are available at <https://doi.org/10.1038/s41561-024-01492-4>.

References

- Burton-Johnson, A., Black, M., Fretwell, P. T. & Kaluza-Gilbert, J. An automated methodology for differentiating rock from snow, clouds and sea in Antarctica from Landsat 8 imagery: a new rock outcrop map and area estimation for the entire Antarctic continent. *Cryosphere* **10**, 1665–1677 (2016).
- Terauds, A. & Lee, J. R. Antarctic biogeography revisited: updating the Antarctic Conservation Biogeographic Regions. *Diversity Distrib.* **22**, 836–840 (2016).
- Green, T. G. A. & Broady, P. in *Biological Soil Crusts: Structure, Function and Management* (eds Belnap, J. & Lange, O. L.) 133–139 (Springer, 2001).
- Davey, M. P. et al. Snow algae communities in Antarctica: metabolic and taxonomic composition. *N. Phytol.* **222**, 1242–1255 (2019).
- Gray, A. et al. Remote sensing reveals Antarctic green snow algae as important terrestrial carbon sink. *Nat. Commun.* **11**, 2527 (2020).
- Robinson, S. A., Wasley, J. & Tobin, A. K. Living on the edge—plants and global change in continental and maritime Antarctica. *Glob. Change Biol.* **9**, 1681–1717 (2003).
- Sancho, L. G., Belnap, J., Colesie, C., Raggio, J. & Weber, B. in *Biological Soil Crusts: An Organizing Principle in Drylands* (eds Weber, B. et al.) 287–304 (Springer, 2016).
- Myers-Smith, I. H. et al. Eighteen years of ecological monitoring reveals multiple lines of evidence for tundra vegetation change. *Ecol. Monogr.* **89**, e01351 (2019).
- Convey, P. et al. The spatial structure of antarctic biodiversity. *Ecol. Monogr.* **84**, 203–244 (2014).
- Chown, S. L. & Convey, P. Spatial and temporal variability across life's hierarchies in the terrestrial Antarctic. *Philos. Trans. R. Soc. Lond. B Biol. Sci.* **362**, 2307–2331 (2007).
- Convey, P. & Biersma, E. M. in *Encyclopedia of Biodiversity* 3rd edn (ed. Scheiner, S. M.) 133–148 (Elsevier, 2024).
- Selkirk, P. M. & Skotnicki, M. L. Measurement of moss growth in continental Antarctica. *Polar Biol.* **30**, 407–413 (2007).
- Green, T. G. A. et al. Flora and vegetation of Cape Hallett and vicinity, northern Victoria Land, Antarctica. *Polar Biol.* **38**, 1825–1845 (2015).
- Parnikoza, I. et al. Current status of the Antarctic herb tundra formation in the Central Argentine Islands. *Glob. Change Biol.* **15**, 1685–1693 (2009).
- Colesie, C. et al. The longest baseline record of vegetation dynamics in Antarctica reveals acute sensitivity to water availability. *Earth's Future* **10**, e2022EF002823 (2022).
- Wasley, J. et al. Bryophyte species composition over moisture gradients in the Windmill Islands, East Antarctica: development of a baseline for monitoring climate change impacts. *Biodiversity* **13**, 257–264 (2012).
- Cannone, N., Malfasi, F., Favero-Longo, S. E., Convey, P. & Guglielmin, M. Acceleration of climate warming and plant dynamics in Antarctica. *Curr. Biol.* **32**, 1599–1606 (2022).
- Hughes, K. A., Ireland, L. C., Convey, P. & Fleming, A. H. Assessing the effectiveness of specially protected areas for conservation of Antarctica's botanical diversity. *Conserv. Biol.* **30**, 113–120 (2015).
- Wauchope, H. S., Shaw, J. D. & Terauds, A. A snapshot of biodiversity protection in Antarctica. *Nat. Commun.* **10**, 946 (2019).
- Leihy, R. I. et al. Antarctica's wilderness fails to capture continent's biodiversity. *Nature* **583**, 567–571 (2020).
- Turner, J. et al. Absence of 21st century warming on Antarctic Peninsula consistent with natural variability. *Nature* **535**, 411–415 (2016).
- Vignon, É., Roussel, M.-L., Gorodetskaya, I. V., Genthon, C. & Berne, A. Present and future of rainfall in Antarctica. *Geophys. Res. Lett.* **48**, e2020GL092281 (2021).
- Colesie, C., Walshaw, C. V., Sancho, L. G., Davey, M. P. & Gray, A. Antarctica's vegetation in a changing climate. *WIREs Clim. Change* **14**, e810 (2022).
- Lee, J. R. et al. Climate change drives expansion of Antarctic ice-free habitat. *Nature* **547**, 49–54 (2017).

25. Fonseca, E. L. D., Santos, E. C. D., de Figueiredo, A. R. & Simoes, J. C. The use of sentinel-2 imagery to generate vegetation maps for the Northern Antarctic Peninsula and offshore islands. *An. Acad. Bras. Ciênc.* **95**, e20230710 (2023).
26. Sotille, M. E. et al. Evaluation of UAV and satellite-derived NDVI to map maritime Antarctic vegetation. *Appl. Geogr.* **125**, 102322 (2020).
27. Singh, C. P. et al. Mapping lichen abundance in ice-free areas of Larsemann hills, East Antarctica using remote sensing and lichen spectra. *Polar Sci.* **38**, 100976 (2023).
28. Fretwell, P. T., Convey, P., Fleming, A. H., Peat, H. J. & Hughes, K. A. Detecting and mapping vegetation distribution on the Antarctic Peninsula from remote sensing data. *Polar Biol.* **34**, 273–281 (2011).
29. Casanovas, P., Black, M., Fretwell, P. & Convey, P. Mapping lichen distribution on the Antarctic Peninsula using remote sensing, lichen spectra and photographic documentation by citizen scientists. *Polar Res.* **34**, 25633 (2015).
30. Gray, A. et al. Remote sensing phenology of antarctic green and red snow algae using WorldView Satellites. *Front. Plant Sci.* **12**, 671981 (2021).
31. Hashim, M. et al. Mapping snow-algae in Antarctic Peninsula with multi-temporal satellite remote sensing data. In *Proc. 2016 IEEE International Geoscience and Remote Sensing Symposium (IGARSS) 5221–5224* (IEEE, 2016).
32. Huovinen, P., Ramirez, J. & Gomez, I. Remote sensing of albedo-reducing snow algae and impurities in the Maritime Antarctica. *ISPRS J. Photogramm.* **146**, 507–517 (2018).
33. Fretwell, P. T. & Trathan, P. N. Discovery of new colonies by Sentinel2 reveals good and bad news for emperor penguins. *Remote Sens. Ecol. Conserv.* **7**, 139–153 (2021).
34. Harris, C. M. et al. *Important Bird Areas in Antarctica 2015* (BirdLife International and Environmental Research & Assessment Ltd, 2015).
35. Román, A., Tovar-Sánchez, A., Fernández-Marín, B., Navarro, G. & Barbero, L. Characterization of an Antarctic penguin colony ecosystem using high-resolution UAV hyperspectral imagery. *Int. J. Appl. Earth Obs.* **125**, 103565 (2023).
36. Salvatore, M. R. et al. Counting carbon: quantifying biomass in the McMurdo Dry Valleys through orbital & field observations. *Int. J. Remote Sens.* **42**, 8597–8623 (2021).
37. Power, S. N., Salvatore, M. R., Sokol, E. R., Stanish, L. F. & Barrett, J. E. Estimating microbial mat biomass in the McMurdo Dry Valleys, Antarctica using satellite imagery and ground surveys. *Polar Biol.* **43**, 1753–1767 (2020).
38. Levy, J., Cary, S., Joy, K. & Lee, C. K. Detection and community-level identification of microbial mats in the McMurdo Dry Valleys using drone-based hyperspectral reflectance imaging. *Antarct. Sci.* **32**, 367–381 (2020).
39. Brooks, S. T. *Our Footprint on Antarctica—Buildings, Disturbance Database* (Australian Antarctic Data Centre, 2018); <https://doi.org/10.26179/5dc8db48eb58e>
40. Terauds, A. et al. Conservation biogeography of the Antarctic. *Diversity Distrib.* **18**, 726–741 (2012).
41. Terauds, A. et al. *Scientific Committee on Antarctic Research (SCAR) Antarctic Terrestrial Biodiversity Database, Version 4, Unreleased Data* (Australian Antarctic Data Centre, 2023); <https://doi.org/10.4225/15/59100ba9157f7>
42. Bollard, B., Doshi, A., Gilbert, N., Poirot, C. & Gillman, L. Drone technology for monitoring protected areas in remote and fragile environments. *Drones* **6**, 42 (2022).
43. Seppelt, R. D. et al. Lichen and moss communities of Botany Bay, Granite Harbour, Ross Sea, Antarctica. *Antarct. Sci.* **22**, 691–702 (2010).
44. Power, S. N. et al. Remotely characterizing photosynthetic biocrust in snowpack-fed microhabitats of Taylor Valley, Antarctica. *Sci. Remote Sens.* **9**, 100120 (2024).
45. Shin, J. I., Kim, H. C., Kim, S. I. & Hong, S. G. Vegetation abundance on the Barton Peninsula, Antarctica: estimation from high-resolution satellite images. *Polar Biol.* **37**, 1579–1588 (2014).
46. Sun, X. H., Wu, W. J., Li, X. W., Xu, X. Y. & Li, J. F. Vegetation abundance and health mapping over southwestern Antarctica based on WorldView-2 data and a modified spectral mixture analysis. *Remote Sens.* **13**, 166 (2021).
47. Miranda, V. et al. Monitoring recent changes of vegetation in Fildes Peninsula (King George Island, Antarctica) through satellite imagery guided by UAV surveys. *Sci. Total Environ.* **704**, 135295 (2020).
48. Gilbert, G. E., Early, T. J. & King, H. T. Biological survey of Ellsworth Land Antarctic. *Antarct. J. U. S.* **4**, 95–96 (1969).
49. Lupachev, A. V., Abakumov, E. V., Abramov, A. A., Goryachkin, S. V. & Gilichinsky, D. A. in *The Soils of Antarctica* (ed. Bockheim, J. G.) 183–203 (Springer, 2015).
50. Petzold, D. E. & Goward, S. N. Reflectance spectra of subarctic lichens. *Remote Sens. Environ.* **24**, 481–492 (1988).

Publisher's note Springer Nature remains neutral with regard to jurisdictional claims in published maps and institutional affiliations.

Open Access This article is licensed under a Creative Commons Attribution 4.0 International License, which permits use, sharing, adaptation, distribution and reproduction in any medium or format, as long as you give appropriate credit to the original author(s) and the source, provide a link to the Creative Commons licence, and indicate if changes were made. The images or other third party material in this article are included in the article's Creative Commons licence, unless indicated otherwise in a credit line to the material. If material is not included in the article's Creative Commons licence and your intended use is not permitted by statutory regulation or exceeds the permitted use, you will need to obtain permission directly from the copyright holder. To view a copy of this licence, visit <http://creativecommons.org/licenses/by/4.0/>.

© The Author(s) 2024

Methods

Sentinel-2 dataset

Sentinel-2A/2B surface reflectance data were accessed and analysed in Google Earth Engine⁵¹ using the JavaScript application programming interface to map green vegetation (vascular plants, bryophytes, algae), lichens and green snow algae across Antarctica. Data were retrieved from six multispectral bands ranging from the visible (-490 nm) to short-wave infrared (SWIR; -1610 nm) wavelengths at a spatial resolution of 10 m (B2, B3, B4 and B8) and 20 m (B5, B11). Only imagery south of 60° S was considered for mapping the vegetation, to maintain consistency with relevant large-scale biogeography and conservation studies across Antarctica^{2,19,20}, and to align with the provisions of the Antarctic Treaty. This imagery covers most of the maritime Antarctic (except for the South Sandwich Islands at 55–60° S and Bouvetøya at 54° S), and the continental Antarctic (except for Scott Island off the northeast coast of Victoria Land, which did not have usable imagery). The sub-Antarctic islands north of the maritime Antarctic contain additional vegetation types that are otherwise absent from the maritime and continental Antarctic, such as ferns and club mosses¹¹. To achieve a Sun-synchronous orbit, Sentinel-2A/2B do not pass directly over the poles. Consequently, a data-void ‘polar hole’ exists south of 82.8° S in Sentinel-2 imagery (Fig. 2). This accounted for ~21% of Antarctica’s total ice-free area estimate (45,886 km²), based on the high-resolution rock outcrop layer from the SCAR Antarctic Digital Database (ADD) Version 7.0 (<http://www.add.scar.org/>), and included the southernmost ice-free areas of the Transantarctic Mountain and Pensacola Mountain bioregions (Fig. 3). Any vegetation present in these ice-free areas could not be detected, although known vegetation in these areas is extremely limited and unlikely to be detected at the resolution available for this study⁵². The rock outcrop layer also included South Georgia (sub-Antarctic), which was not mapped in this study. The combined ice-free area contained within the polar hole and on South Georgia, calculated from the ADD high-resolution rock outcrop layer, were subtracted from the initial total area estimate (45,886 km²), leaving around 35,082 km² remaining for comparative area analysis.

Remote sensing of Antarctic vegetation

Terrestrial vegetation. The major vegetation types that grow in Antarctica’s ice-free areas include vascular plants, mosses, lichens, algae and cyanobacteria. Based on spectral similarity⁵³, the terrestrial vegetation was subdivided into green vegetation (vascular plants, bryophytes and green algae) and lichens for classification in Sentinel-2 imagery. To prepare for vegetation classification, level-2A Sentinel-2 imagery was retrieved over Antarctica’s ice-free areas. The image search area was restricted to an ~10-km buffer around ice-free areas. Within the resulting search area, imagery was selected over five consecutive austral summer seasons (December–February from 2018 to 2023) to maximize the availability of cloud-free scenes over ice-free areas. Imagery within this date range was removed if the cloud pixel percentage across the entire image tile (110 × 110 km) exceeded 82%. We kept the cloud threshold high to prevent filtering out substantial areas of cloud-free bare ground pixels in the large image tiles if they had high net cloud-cover percentages. Additionally, imagery was removed if the solar zenith angle exceeded 70° (<https://sentinel.esa.int/web/sentinel/technical-guides/sentinel-2-msi/data-quality-reports>). To remove ocean from the analysis, all images were masked according to the high-resolution sea mask in the Quantarctica dataset⁵⁴. In total, just under 82,000 Sentinel-2 scenes over ice-free areas remained for further analysis. To keep the mapping methodology as reproducible as possible, no manual quality control was carried out on the imagery. Instead, the final vegetation map relied on successful masking to remove poor-quality pixels, although this could not be guaranteed in every case. We used Google Earth Engine’s Scene Classification Layer (SCL) map at 20-m resolution together with multispectral band ratio indices to mask pixels of potential false positives. This included snow

and ice, water, topographic and cloud-cast shadows, dark near-infrared (NIR) features and remaining cloud. We also masked regions above 500 m using the 8-m mosaic Reference Elevation Model for Antarctica (REMA)⁵⁵, to provide a spatial constraint for analysis and reduce inland false positives from complex mountainous topography (which has a strong impact on NDVI values due to distortion⁵⁶). This cutoff was based on in situ observations of vegetation elevation limits^{57,58}. However, we acknowledge that this may reduce the map’s applicability in inland and high mountain areas and could result in an underestimate of the total area of vegetation across Antarctica. Future work should incorporate higher elevation areas, and the code presented may be adapted to run over smaller areas where topographic effects may be controlled. For example, Fig. 5a shows an area of the Hudson mountains where we have locally set an elevation limit of 1,300 m on Webber Nunatak and Meyers Nunatak, increasing the detection of green vegetation in this region by 612 m². After masking, usable imagery was estimated to be available for over 98.42% of the ice-free area, with discrete patches of cloudy or saturated pixels obscuring 867 km² of land from analysis.

To detect and discriminate green vegetation and lichens in remaining pixels from the multi-temporal Sentinel-2 images, the NDVI was computed (equation (1)) in conjunction with the normalized difference moisture index (NDMI; equation (2)):

$$\text{NDVI} = \frac{\text{NIR} - \text{Red}}{\text{NIR} + \text{Red}} \quad (1)$$

NDVI uses the red band (B4) and NIR band (B8) at 10-m resolution in Sentinel-2 imagery to infer the greenness of vegetation. This index was used to aid in the discrimination of green vegetation and lichen, based on their different spectral responses across these bands⁵³, resulting in generally higher values for green vegetation and lower values for lichens (Extended Data Table 2 and Supplementary Table 1). Brown mosses (Figs. 1e and 5b) should have sufficiently high NDVI values for detection in our model (Supplementary Table 1), as long as the patch size is above minimum detection limits (Table 1). However, grey or black mosses (Fig. 5f) are unlikely to have sufficiently high reflectance in visible wavelengths for detection in our model. We used relatively high minimum NDVI thresholds for classification to minimize the chance of false positives from rock, which tends to have comparatively low NDVI values (Supplementary Table 1), akin to pixels containing sparse vegetation coverage²⁸. Consequently, this approach meant that sparse vegetation within pixels dominated by bare ground could not be detected (Table 1). Cyanobacterial mats were intentionally not mapped with this methodology, yet some communities with confirmed presence were detected in the map. Typical submergence in meltwater streams and ponds, in addition to differing mat colour (orange/brown or black), contributes to their ability to exhibit both sufficiently high NDVI values within the detection thresholds of our classification^{37,59} (Supplementary Table 1), in addition to relatively low NDVI values that we were unable to discriminate from bare ground.

The second index used for classification, NDMI, makes use of the NIR and SWIR (B11) bands at 10-m and 20-m resolutions, respectively. This index is used to infer the moisture content of vegetation based on changes in SWIR reflectance, and was originally designed to complement the use of NDVI for the remote sensing of vegetation⁶⁰. NDMI has not previously been used for mapping vegetation across Antarctica, yet numerous studies have recognized the potential of using vegetation water content (affecting SWIR reflectance) in remote sensing^{53,61,62}. Antarctic vegetation can experience extreme fluctuations in water content on a diurnal basis⁶³, making NDMI a particularly useful index for remote detection:

$$\text{NDMI} = \frac{\text{NIR} - \text{SWIR}}{\text{NIR} + \text{SWIR}} \quad (2)$$

During a field campaign to Robert Island in early 2023 (Supplementary Table 2), in situ spectral reflectance measurements

of representative moss and lichen morphotypes were obtained on a weekly basis over the field season, using a Spectral Evolution PSR + 3500 field spectrometer (Supplementary Table 1). The spectra convolved to the bands of Sentinel-2 demonstrated that, under image-acquisition conditions (cloud-free, sunny skies), lichens on average exhibited negative NDMI values, implying dehydration (Supplementary Table 1). Conversely, mosses exhibited both positive (hydrated) and negative (dehydrated) NDMI values (Supplementary Table 1). This could possibly be explained by differing rates of dehydration at the onset of intense solar radiation, whereby lichens dehydrate rapidly⁶⁴ based on some combination of general morphological variations (lichens tend to have high surface area-to-volume ratios⁶⁵), colour (darker coloured lichens will absorb light energy, warm and dehydrate more rapidly^{50,63}), physical attachment to the underlying substrate and habitat preference (lichens generally can be found in more xeric (dry) locations and mosses in both xeric and hydric (wet) locations^{64,66}). As a result, based on the assumption of dehydration in at least one image over our acquisition period, we used negative NDMI to detect lichens in the Sentinel-2 imagery. We also incorporated a wider NDMI threshold range for green vegetation to encompass both hydrated and dehydrated species in the model. Although bare ground can exhibit relatively low NDMI values similar to dehydrated lichens and green vegetation, it also typically displays lower NDVI values (Supplementary Table 1). Therefore, the synergy between indices was key in enhancing the discrimination potential of each class. The effect of water content on the NDMI values of Antarctic terrestrial vegetation species was tested further through hydration- and dehydration-induced spectral reflectance experiments in the laboratory, using the ASD FieldSpec3 (Malvern Panalytical) and Spectral Evolution PSR + 3500 (Supplementary Table 1) set-ups. The green red vegetation index (GRVI) and the normalized difference red edge (NDRE) index were additionally used for lichen classification (Extended Data Table 2), to help reduce the likelihood of rock false positives. Our Sentinel-2 convolved spectral analyses were used to assess spatial and temporal variations in spectral index values across the summer season, there by assisting in the class discrimination for lichen and green vegetation (Extended Data Table 2 and Supplementary Table 1).

After the green vegetation and lichen had been identified in the available image pixels, a mean composite map was generated for each vegetation type across Antarctica's ice-free areas. These composite maps were then exported from Google Earth Engine. To further reduce remaining false positives in the vegetation maps, both were clipped in QGIS software (version 3.16.9) to the Landsat 8 rock outcrop layer¹ (buffered by 250 m to include ice-free areas that were masked in the layer). This rock outcrop buffer zone encompasses the ice-free areas from the ADD high-resolution rock outcrop layer.

Cryospheric vegetation. Green snow algal blooms were identified within the Sentinel-2 imagery by adapting our previous approach⁵ for use in Google Earth Engine. For this, level-2A Sentinel-2 imagery with less than 20% cloud cover was used from five consecutive summer seasons (December–February from 2017 to 2022). The spatial distribution of these scenes is visualized in Supplementary Fig. 1. The search area for imagery was constrained to an 80-km buffer either side of the Quantarctica high-resolution coastline layer⁵⁴. A larger search area for green snow algae resulted in usable imagery from December 2017, but this imagery was not available over ice-free areas for the terrestrial vegetation mapping. Ocean pixels were first clipped out using a modified version of the ADD SeaMask, which had been extended 100 m out to sea. The remaining ocean was then masked using a minimum reducer on the SCL band and removing areas with pixels classified as water. We opted for this approach over clipping to the ADD SeaMask, as the geolocation mismatch between Sentinel-2 images and the sea mask excluded many shoreline snow patches and narrow peninsulas from analysis. To reduce false positives, pixels were also masked if

they exceeded an elevation of 500 m (based on a maximum observed in situ bloom elevation of ~100 m on Robert Island, 2023) and did not have snow/ice classification in the SCL band, by using the masking functions described in equation (3). After masking, we used the scaled integral of B4 to B3 and B5 (I_{B4} ; equation (4))⁵ to estimate the relative amount of chlorophyll within each pixel. This was then related to cell densities using the empirical relationship between in situ cell density and I_{B4} (equation (5))⁵:

$$(B2 \geq B5) \text{OR} (B2 > B3) \text{OR} (B2 > 1) \text{OR} (B11 > 0.15) \text{OR} \\ (B2 < 0.3 \text{ AND } B8 < 0.25) \text{OR} (B8 < B8a) \text{OR} (B4 > B5) \quad (3)$$

$$I_{B4} = \frac{R_{B3}(\lambda_{B5}-\lambda_{B4})+R_{B5}(\lambda_{B4}-\lambda_{B3})}{\lambda_{B5}-\lambda_{B3}} \\ -R_{B4} \frac{R_{B3}(\lambda_{B5}-\lambda_{B4})+R_{B5}(\lambda_{B4}-\lambda_{B3})}{\lambda_{B5}-\lambda_{B3}} \quad (4)$$

$$\text{Green cells ml}^{-1} = (I_{B4} \times 302,067) + 4,393 \quad (5)$$

We used a maximum reducer to composite our image collection into a single raster layer, whereby any location within the search area that was identified as containing green snow algae over the entire search period was classified as green snow algae. For areas where green snow algae were identified in the same location within multiple images, the reducer returned the maximum estimated cell density for that pixel. To further reduce false positives in our analysis, we filtered out pixels containing fewer than 15,000 cells ml⁻¹ estimated cell density. We chose a higher threshold than our previous work⁵ due to the substantially larger number of images being analysed. Output noise was reduced using a 7 × 7 circular kernel filter with a minimum reducer to mask out isolated pixels. The resulting layer was exported for further analysis and combined (using a union function to remove overlap) with the data from our previous analysis⁶⁷. Zonal statistics (Fig. 2) and bioregion analyses (Fig. 3) on the final cryospheric and terrestrial vegetation maps were carried out using QGIS software.

Estimating minimum detection limits and lower area bounds

To determine the minimum area that each vegetation class could occupy in a Sentinel-2 pixel for detection with the respective classification thresholds, we calculated mean NDVI, NDMI, GRVI, NDRE and I_{B4} values from our Sentinel-2 convolved reflectance spectra of green vegetation ($n = 7$), lichen ($n = 17$), rock ($n = 21$), green snow algae ($n = 91$) and clean snow ($n = 15$) samples (Supplementary Table 1). Using Python in Jupyter Notebook (version 6.4.6), we randomly generated 1,000 artificial mixtures of green vegetation/rock, lichen/rock and green snow algae/clean snow, respectively, to simulate different proportions in a Sentinel-2 pixel. Weighted mean index values were then calculated for our respective simulated Sentinel-2 pixels, and plotted against the artificial mixture proportions. We then determined the lowest abundance of each vegetation type that could occupy a Sentinel-2 pixel while satisfying the classification thresholds (Extended Data Table 2). The resulting values were used as the minimum areas for detection (Table 1). The calculations for each vegetation type did not account for the point spread function, and they assumed uniform reflectance across a pixel and that no other vegetation type was present within the pixel (other than bare ground for terrestrial vegetation and clean snow for green snow algae, as demonstrated in Fig. 1a,c). Classification uncertainty arising from mixed vegetation pixels (Fig. 1e) will require further spectral mixture analysis. Our minimum abundance estimates represent approximations, and could vary based on rock type, species, colour and hydration status. Finally, the binary classifiers used in this study assume that detected vegetation covers the entirety of a given Sentinel-2 pixel, which is often not the case with Antarctica's sparse and spatially patchy vegetation. We estimated the lower bound of total

area estimates for green vegetation, lichens and green snow algae by multiplying the minimum area for detection estimates for each type (Table 1) by the total number of vegetation pixels detected in each composite map ($n = 328,312$, $n = 81,422$ and $n = 32,629$, respectively). We then converted units from square metres to square kilometres.

Ground validation

Ground validation data for vegetation were assessed at the same spatial resolution as Sentinel-2 (10×10 m), to ensure spatially comparable data. Green vegetation, lichen and bare ground validation sites ($n = 455$) were acquired from true-colour high-resolution (sub-decimetres) UAV imagery and classified maps from the published literature^{26,37,38,68–82}; Global Positioning System (GPS) tagged digital photographs; GPS tracks over Léonie Island ($67^\circ 35' S$ $68^\circ 19' W$) and Anchorage Island ($67^\circ 36' S$ $68^\circ 12' W$) in Ryder Bay, Antarctic Peninsula from February 2007⁸³; and a dGPS survey using an Emlid Reach RS + GNSS receiver (Fig. 1c,d) operated in RTK mode with a base station over Robert Island ($62^\circ 24' S$ $59^\circ 30' W$), South Shetland Islands, visited by the authors from 1 January 2023 to 24 February 2023 (Extended Data Fig. 1 and Supplementary Table 2). Just under 10% of the validation data were obtained from sites within 5 km of IBAs³⁴. For the Hudson Mountains ($72^\circ 25' S$ $99^\circ 30' W$; Fig. 5a), ground validation data were based on opportunistic ground-based observations, photographs and GPS location measurements (using a Javad Triumph II receiver) made during a geological field campaign undertaken by one of the authors (J.S.J.) from 25 November to 31 December 2019. For the green snow algae, validation sites ($n = 256$) were acquired from field observations made by the authors over the austral summer season at Rothera Point ($67^\circ 34' S$, $68^\circ 07' W$) and islands around Ryder Bay ($67^\circ 36' S$, $68^\circ 16' W$) in 2018, King George Island in 2019 ($62^\circ 10' S$ $58^\circ 53' W$) and Robert Island ($62^\circ 24' S$ $59^\circ 30' W$) in 2023; observations from a cruise along the Antarctic Peninsula on the RRS *Sir David Attenborough* between Rothera Research Station and King George Island (December 2022); Antarctic Peninsula cruise observations from Hanna Michel; observations from participants of the Homeward Bound expedition and from published literature^{4,84–90}, where fieldwork was completed between 2017 and 2022 (Extended Data Fig. 1 and Supplementary Table 2). Over 60% of the terrestrial and cryospheric validation data were obtained from the South Shetland Islands, where over 50% of all vegetation was detected.

There was a 3-year gap between the first available cloud-free Sentinel-2 image over Robert Island (2019) and the ground validation data, and a 16-year gap between cloud-free imagery over Léonie and Anchorage Island (2023) and the ground validation data. Vegetation growth and decline is considered to have had no influence on the accuracy assessment, based on relatively slow vegetation growth rates documented across the maritime Antarctic^{91,92}. Ground validation data from the published literature and GPS-tagged photographs were manually digitized as polygons in QGIS software over Sentinel-2 true-colour composites. The GPS validation sites from Ryder Bay and Robert Island were uploaded and re-projected to match the vegetation layers (EPSG: 3031), also in QGIS software. All validation polygons were given a classification of green vegetation, lichen or bare ground based on notes and photographs taken during the ground validation surveys. An accuracy assessment was then carried out on the terrestrial vegetation map using the classified ground validation data (Extended Data Fig. 1) and Cohen's kappa statistic.

Data availability

The green vegetation, lichen and green snow algae maps generated during the current study are available in the figshare repository, with the identifier <https://doi.org/10.6084/m9.figshare.24745956> (ref. 93). The spectral library dataset supporting Extended Data Table 2 and Supplementary Table 1 is available in the Edinburgh DataShare repository, with the identifier <https://doi.org/10.7488/ds/7720> (ref. 94).

Code availability

The JavaScript code for generating the green vegetation, lichen and green snow algae maps in Google Earth Engine are available in the GitHub repository, with the identifier <https://doi.org/10.5281/zenodo.11264049> (ref. 95).

References

- Gorelick, N. et al. Google Earth Engine: planetary-scale geospatial analysis for everyone. *Remote Sens. Environ.* **202**, 18–27 (2017).
- Hodgson, D. A. et al. The limnology and biology of the Dufek Massif, Transantarctic Mountains 82° South. *Polar Biol.* **4**, 103–113 (2010).
- Haselwimmer, C. & Fretwell, P. Field reflectance spectroscopy of sparse vegetation cover on the Antarctic Peninsula. In *Proc. 2009 First Workshop on Hyperspectral Image and Signal Processing: Evolution in Remote Sensing 1–4* (IEEE, 2009).
- Matsuoka, K. et al. Quantarctica [Data set]. *Norwegian Polar Institute* <https://doi.org/10.21334/npolar.2018.8516e961> (2018).
- Howat, I. M., Porter, C., Smith, B. E., Noh, M. J. & Morin, P. The Reference Elevation Model of Antarctica. *Cryosphere* **13**, 665–674 (2019).
- Chen, F., Muramoto, K.-I. & Kubo, M. Calculation of NDVI in mountainous areas. In *Scanning the Present and Resolving the Future. Proc. IEEE 2001 International Geoscience and Remote Sensing Symposium 2340–2342* (IEEE, 2001).
- Cannone, N., Fratte, M. D., Convey, P., Worland, M. R. & Guglielmin, M. Ecology of moss banks at Signy Island (maritime Antarctica). *Bot. J. Linn. Soc.* **184**, 518–533 (2017).
- Colesie, C., Büdel, B. & Green, T. G. A. Endolithic communities in the McMurdo Dry Valleys: biomass, turnover, cyanobacteria and location – a preliminary insight. *Algol. Stud.* **151/152**, 51–68 (2016).
- Salvatore, M. R. et al. Remote characterization of photosynthetic communities in the Fryxell basin of Taylor Valley, Antarctica. *Antarct. Sci.* **32**, 255–270 (2020).
- Gao, B. NDWI—a normalized difference water index for remote sensing of vegetation liquid water from space. *Remote Sens. Environ.* **58**, 257–266 (1996).
- Fonseca, E. L., Santos, E. C. D., Figueiredo, A. R. D. & Simoes, J. C. Antarctic biological soil crusts surface reflectance patterns from Landsat and Sentinel-2 images. *Ann. Braz. Acad. Sci.* **94**, e20210596 (2022).
- Granlund, L., Keski-Saari, S., Kumpula, T., Oksanen, E. & Keinanen, M. Imaging lichen water content with visible to mid-wave infrared (400–5,500 nm) spectroscopy. *Remote Sens. Environ.* **216**, 301–310 (2018).
- Bartak, M. et al. Inhibition of primary photosynthesis in desiccating Antarctic lichens differing in their photobionts, thallus morphology and spectral properties. *Microorganisms* **9**, 818 (2021).
- Green, T. G. A., Sancho, L. G. & Pintado, A. in *Plant Desiccation Tolerance. Ecological Studies* Vol. 215 (eds Lüttge, U. et al.) 89–120 (Springer, 2011).
- Lakatos, M. in *Plant Desiccation Tolerance. Ecological Studies* Vol. 215 (eds Lüttge, U. et al.) 65–87 (Springer, 2011).
- Schroeter, B., Green, T. G. A., Pintado, A., Tuerk, R. & Sancho, L. G. Summer activity patterns for mosses and lichens in Maritime Antarctica. *Antarct. Sci.* **29**, 517–530 (2017).
- Gray, A. et al. Green snow algae remote sensing metadata. *figshare* <https://doi.org/10.6084/m9.figshare.c.4893771.v1> (2020).
- Robinson, S. A. et al. Rapid change in East Antarctic terrestrial vegetation in response to regional drying. *Nat. Clim. Change* **8**, 879–884 (2018).
- Tovar-Sanchez, A., Roman, A., Roque-Atienza, D. & Navarro, G. Applications of unmanned aerial vehicles in Antarctic environmental research. *Sci. Rep.* **11**, 21717 (2021).

70. Ruiz-Fernández, J., Oliva, M. & García-Hernández, C. Topographic and geomorphologic controls on the distribution of vegetation formations in Elephant Point (Livingston Island, Maritime Antarctica). *Sci. Total Environ.* **587–588**, 340–349 (2017).
71. Zmarz, A. et al. Application of UAV BVLOS remote sensing data for multi-faceted analysis of Antarctic ecosystem. *Remote Sens. Environ.* **217**, 375–388 (2018).
72. Zmarz, A. et al. BVLOS UAV missions for vegetation mapping in maritime Antarctic. *Front. Environ. Sci.* **11**, 1154115 (2023).
73. Zmarz, A., Korczak-Abshire, M., Storbvold, R., Rodzewicz, M. & Kedzierska, I. Indicator species population monitoring in Antarctica with UAV. *Int. Arch. Photogramm. Remote Sens. Spatial Inf. Sci.* **XL-1/W4**, 189–193 (2015).
74. Poelking, E. L., Schaefer, C. E. R., Fernandes Filho, E. I., de Andrade, A. M. & Spielmann, A. A. Soil-landform-plant-community relationships of a periglacial landscape on Potter Peninsula, maritime Antarctica. *Solid Earth* **6**, 583–594 (2015).
75. Sotille, M. E. et al. UAV-based classification of maritime Antarctic vegetation types using GEOBIA and random forest. *Ecol. Inform.* **71**, 101768 (2022).
76. Turner, D. J., Malenovsky, Z., Lucieer, A., Turnbull, J. D. & Robinson, S. A. Optimizing spectral and spatial resolutions of unmanned aerial system imaging sensors for monitoring antarctic vegetation. *IEEE J. Stars* **12**, 3813–3825 (2019).
77. Malenovsky, Z., Lucieer, A., King, D. H., Turnbull, J. D. & Robinson, S. A. Unmanned aircraft system advances health mapping of fragile polar vegetation. *Methods Ecol. Evol.* **8**, 1842–1857 (2017).
78. Lucieer, A., Robinson, S. & Turner, D. High resolution mapping of moss beds at ASPA 135, Robinson Ridge and near the Red Shed at Casey, January 2010, Ver. 1. *Aust. Antarct. Data Cent.* <https://doi.org/10.4225/15/55B81E9BA3649> (2015).
79. Lucieer, A., Robinson, S. A., Turner, D. & Malenovsky, Z. Unmanned Aircraft Systems (UAS) remote sensing datasets for ASPA135, Robinson Ridge and Red Shed, Ver. 1. *Aust. Antarct. Data Cent.* <https://doi.org/10.4225/15/555D755E50DB8> (2015).
80. Lucieer, A., Robinson, S. & Turner, D. Using an unmanned aerial vehicle (UAV) for ultra-high resolution mapping of Antarctic moss beds. In *Proc. 15th Australasian Remote Sensing & Photogrammetry Conference* 1–12 (School of Geography & Environmental Studies, 2010).
81. Poeiras, L. M. *Vegetation and Environments in Lions Rump and Hope Bay, Maritime Antarctic* (Federal Univ. Viçosa, 2011).
82. Wilkins, D., Spedding, T. & McWatters, R. Orthomosaic and digital surface model of Casey station, 10th February 2022, Ver. 1. *Aust. Antarct. Data Cent.* <https://doi.org/10.26179/4bw4-7n53> (2023).
83. Peat, H. Mapping of the extent of vegetation patches on Leonie and Anchorage Islands in Ryder Bay, Antarctica in 2007 (Version 1.0) [Data set]. *NERC EDS UK Polar Data Cent.* <https://doi.org/10.5285/8a885e6c-3a27-4cd7-850a-1ac1b9f89576> (2023).
84. Procházková, L., Leya, T., Křížková, H. & Nedbalová, L. *Sanguina nivaloides* and *Sanguina aurantia* gen. et spp. nov. (Chlorophyta): the taxonomy, phylogeny, biogeography and ecology of two newly recognised algae causing red and orange snow. *FEMS Microbiol. Ecol.* **95**, fiz064 (2019).
85. Buda, J. et al. Biotope and biocenosis of cryoconite hole ecosystems on Ecology Glacier in the maritime Antarctic. *Sci. Total Environ.* **724**, 138112 (2020).
86. Lutz, S., Ziolkowski, L. A. & Benning, L. G. The biodiversity and geochemistry of cryoconite holes in Queen Maud Land, East Antarctica. *Microorganisms* **7**, 160 (2019).
87. Soto, D. F., Fuentes, R., Huovinen, P. & Gómez, I. Microbial composition and photosynthesis in Antarctic snow algae communities: integrating metabarcoding and pulse amplitude modulation fluorometry. *Algal Res.* **45**, 101738 (2020).
88. Ji, M. et al. Similar heterotrophic communities but distinct interactions supported by red and green-snow algae in the Antarctic Peninsula. *N. Phytol.* **233**, 1358–1368 (2022).
89. Smirnova, M. et al. Isolation and characterization of fast-growing green snow bacteria from coastal East Antarctica. *MicrobiologyOpen* **10**, e1152 (2021).
90. Samui, G., Antony, R. & Thamban, M. Fate of dissolved organic carbon in Antarctic surface environments during summer. *J. Geophys. Res. Biogeosci.* **125**, e2020JG005958 (2020).
91. Sancho, L. G., Green, T. G. A. & Pintado, A. Slowest to fastest: extreme range in lichen growth rates supports their use as an indicator of climate change in Antarctica. *Flora* **202**, 667–673 (2007).
92. Clarke, L. J., Robinson, S. A., Hua, Q., Ayre, D. J. & Fink, D. Radiocarbon bomb strike reveals biological effects of Antarctic climate change. *Glob. Change Biol.* **18**, 301–310 (2012).
93. Walshaw, C. V. & Gray, A. Remote-sensed maps of terrestrial and cryospheric vegetation across Antarctica. *figshare* <https://doi.org/10.6084/m9.figshare.24745956> (2024).
94. Walshaw, C. V., Gray, A. & Colesie, C. Spectral Library of Antarctic Terrestrial Vegetation Species [dataset]. *Univ. Edinb. Sch. Geosci.* <https://doi.org/10.7488/ds/7720> (2024).
95. Walshaw, C. V. & Gray, A. Plantarctica/Antarctic-vegetation-maps: GEE code. *Zenodo* <https://doi.org/10.5281/zenodo.11264049> (2024).

Acknowledgements

For the purpose of open access, we have applied a Creative Commons Attribution (CC BY) licence to any Author Accepted Manuscript version arising from this submission. This research was funded under a joint UKRI NERC and UK Space Agency PhD (SENSE CDT) awarded to C.V.W. (NE/T00939X/1), two UKRI NERC grants NE/V000764/1 and NE/V000896/1 awarded to A.G., P.T.F., P.C., M.P.D. and C.C., and a DEFRA grant (Darwin Plus DPLUS186, Evidence-based conservation of biodiversity in the South Sandwich Islands) awarded to C.C. and P.C. We are especially grateful to the Chilean Antarctic Institute (INACH) for their logistical support for the Robert Island fieldwork in 2023, in particular R. Quinan, D. Haeger, I. Reyes, B. Escare, J. Bravo and A. López Lara. Special thanks go to H. Moulton and T. King, our British Antarctic Survey (BAS) field guides on Robert Island and in the Hudson Mountains. We also thank the staff of the Rothera Research Station, Antarctica, and the crew on the RRS *Sir David Attenborough* (BAS), staff at the Escudero Base on King George Island (INACH), all the logistics and support staff at BAS, and N. Thomas (SAMS), A. Thomson (SAMS), A. Smith (University of Cambridge) and L. Peck (BAS) for wider scientific support. Fieldwork in the Hudson Mountains was undertaken by J.S.J. as part of the Geological History Constraints project, a component of the International Thwaites Glacier Collaboration (ITGC), funded by NERC grant NE/SO06710/1 with logistics provided by the British Antarctic Survey and US Antarctic Program. This is ITGC Contribution No. 124. We thank the NERC Field Spectroscopy Facility (NERC FSF), Edinburgh, for the loan of the ground and UAV spectroscopy equipment (loan references 765.0617, 796.0618, 826.1119, 858.1120, 882.1121 and 898.0522), training in the use of the equipment, and provision of the code for analysing the Spectral Evolution PSR+3500, ASD FieldSpec3 (Malvern Panalytical) and Spectra Vista Corporation (SVC) 1024i data. Thanks go to H. Michel, the Homeward Bound Expeditions members (H. Laeverenz Schlogelhofer, D. Hessenberger, K. R. Duncan), T. Contador (University of Magallanes) and E. Vega (INACH) for snow algae validation data. A UAV orthomosaic of Rothera, used for validation, was collected by The Mapping and Geographic Information Centre (MAGIC) at BAS. Livingston Island fieldwork (contributing to Supplementary Table 1) was supported by a grant from the Spanish Ministry of Science (CRYPTOCOVER, CTM2015-64728-C2-1-R and POLAR-ROCKS,

PID2019-105469RB-C21). We thank T. Wade, manager of the Airborne Research and Innovation facility within the School of Geosciences, University of Edinburgh, for providing UAV training and support. Cape Hallett and Botany Bay fieldwork was supported by the Resilience in Antarctic Biota and Ecosystems Project, funded by the New Zealand Antarctic Research Institute (NZARI 2016-2), and the Dry Valley Ecosystem Resilience (DryVER) programme, funded by the New Zealand Ministry of Business, Innovation and Employment (UOWX1401). Validation sites at Rothera (2018) and King George Island (2019) were funded by a Leverhulme Trust Research Grant (RPG-2017-077) awarded to M.P.D. and P.C.

Author contributions

A.G., C.V.W., P.C., M.P.D. and C.C. designed the study. C.V.W. and A.G. developed the remote-sensed maps and carried out the geospatial analyses and validation. C.V.W., A.G., M.P.D. and C.C. planned the fieldwork and logistics on Robert Island. C.V.W., A.G., M.P.D., C.C., P.T.F., P.C. and J.S.J. carried out the fieldwork. C.V.W. led the writing of the manuscript, with all authors contributing and editing the text. All authors have seen and approved the final version.

Competing interests

The authors declare no competing interests.

Additional information

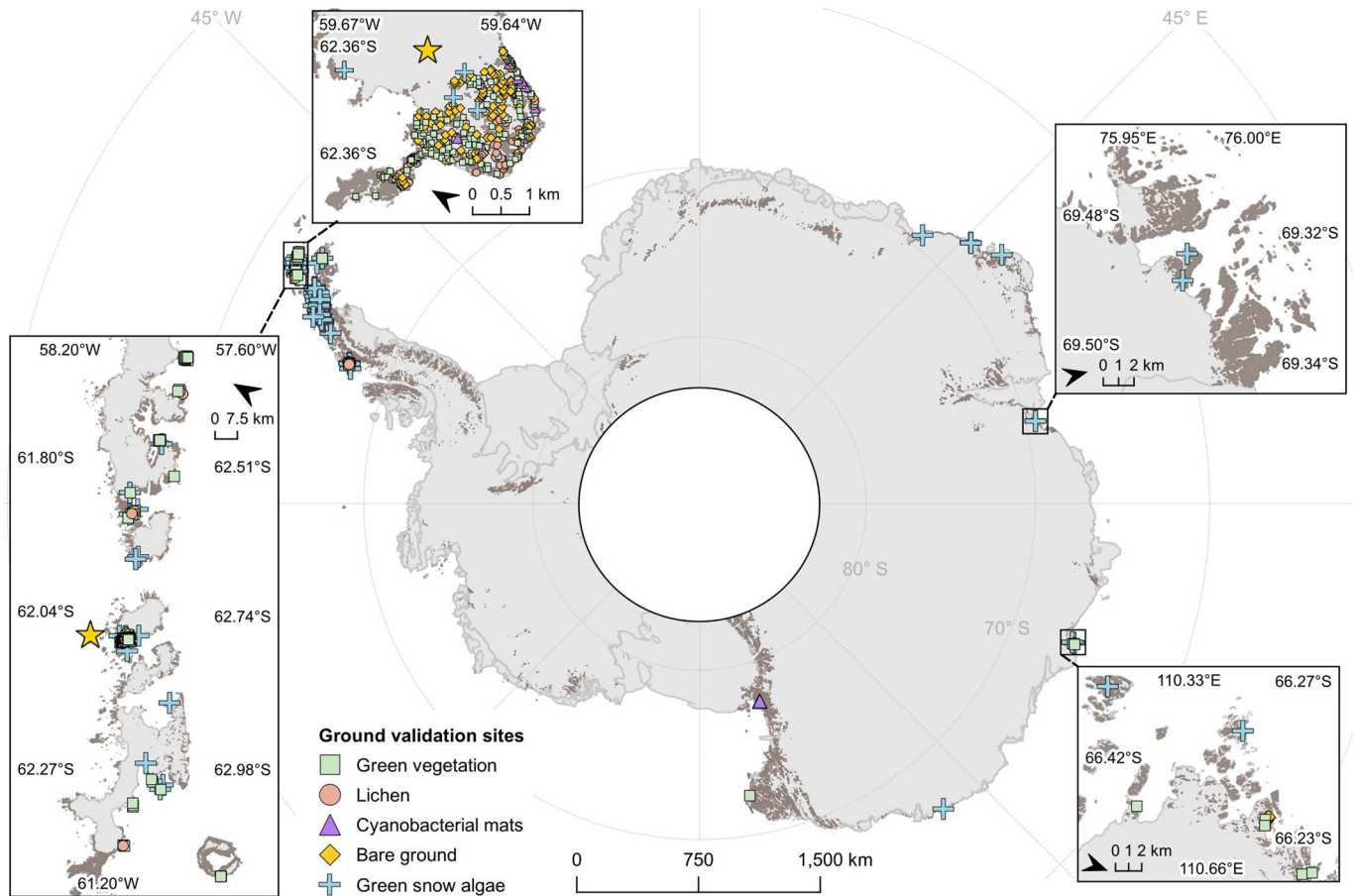
Extended data is available for this paper at <https://doi.org/10.1038/s41561-024-01492-4>.

Supplementary information The online version contains supplementary material available at <https://doi.org/10.1038/s41561-024-01492-4>.

Correspondence and requests for materials should be addressed to Charlotte V. Walshaw, Andrew Gray or Claudia Colesie.

Peer review information *Nature Geoscience* thanks Nicolas Lecomte and Sarah Power for their contribution to the peer review of this work. Primary Handling Editor: Xujia Jiang, in collaboration with the *Nature Geoscience* team.

Reprints and permissions information is available at www.nature.com/reprints.



Extended Data Fig. 1 | Sentinel-2 ground validation sites across Antarctica (not to scale). Each ground validation site was assessed and classified at a 10×10 m scale, corresponding to a Sentinel-2 pixel. Top left inset: Robert Island. Bottom left: South Shetland Islands (yellow star denotes the location of Robert

Island). Top right: Larsemann Hills. Bottom right: Windmill Islands. The base map and ice-free area (dark grey) layer were retrieved from the Antarctic Digital Database Version 7.0.

Extended Data Table 1 | Vegetation area (km²) in bioregions

Bioregion	Area (km ²)			Sum	Percentage of total vegetation
	Green vegetation	Lichen	Green snow algae		
South Shetland Islands	18.3023	5.372	0.5137	24.1881	54.6793
North Antarctic Peninsula	3.4877	0.8995	1.2981	5.6853	12.852
South Orkney Islands	3.1359	1.1195	n/a*	4.2554	9.6198
North-east Antarctic Peninsula	1.6308	0.4093	0.0947	2.1349	4.8261
North Victoria Land	1.3342	0.0317	0.0971	1.463	3.3074
Prince Charles Mountains	1.0889	0.0517	0.0684	1.209	2.733
South Victoria Land	1.0513	0.0582	0.0455	1.1551	2.6112
Thala Hills/Syowa	0.8222	0.0191	0.3023	1.1437	2.5854
Bunger Hills	0.6026	0.0006	0.1027	0.706	1.5959
South Antarctic Peninsula	0.2511	0.1265	0.1941	0.5718	1.2925
East Antarctic Peninsula	0.3882	0.0027	0.119	0.5099	1.1527
Vestfold Hills	0.3148	0.0108	0.033534	0.3592	0.812
Marie Byrd Land	0.2026	0.0031	0.0475	0.2532	0.5723
Windmill Islands	0.0497	0.0133	0.1033	0.1664	0.3763
Ellsworth Land	0.0019	0.0002	0.1074	0.1095	0.2477
Transantarctic Mountains	0.0893	0.0002	0	0.0895	0.2023
Commonwealth Bay	0.0062	0.0016	0.0789	0.0866	0.1959
Eights Coast/Thurston Island	0.043	0.0004	0.0154	0.0588	0.133
Alexander Island	0.0194	0.0182	0.0016	0.0393	0.0889
Dronning Maud Land	0.0019	0.0004	0.0199	0.0223	0.0504
Pensacola Mountains	0.0002	0.0006	0.0188	0.0196	0.0443
Balleny Islands	0.0062	0	0.0007	0.007	0.0158
Ellsworth Mountains	0.0003	0.0022	0	0.0025	0.0056
Total	32.8312	8.1422	3.2629	44.2362	

*There was no data available for green snow algae over the South Orkney Islands due to a lack of imagery with < 20% cloud cover during the search period (2017–2022).

Extended Data Table 2 | Spectral reflectance index threshold values used for vegetation classification

Spectral reflectance index	Multispectral bands (spatial resolution, m)	Threshold ranges		
		Green vegetation (vascular plants, bryophytes, green algae)	Lichen	Green snow algae (cells ml ⁻¹)
NDVI	B8 (10), B4 (10)	0.4 – 0.98	0.2 – 0.4	n/a
NDMI	B8 (10), B11 (20)	-0.2 – 0.6	-0.05 – -0.2	n/a
GRVI	B3 (10), B4 (10)	n/a	> -0.05	n/a
NDRE	B8 (10), B5 (20)	n/a	> 0.1	n/a
I_{B4}	B3 (10), B4 (10), B5 (20)	n/a	n/a	> 15,000